Binder-free textile PAN-based electrodes for aqueous-based and glycerol-based supercapacitors

Ingrid Ariani Belineli Barbosa (ibelineli.93@gmail.com)
IPEN: Instituto de Pesquisas Energeticas e Nucleares https://orcid.org/0000-0002-5316-9518
Jossano Saldanha Marcuzzo
INPE: Instituto Nacional de Pesquisas Espaciais
Rubens Nunes de Faria Jr
IPEN: Instituto de Pesquisas Energeticas e Nucleares
Ivana Conte Consentino
IPEN: Instituto de Pesquisas Energeticas e Nucleares

Research Article

Keywords: Supercapacitors, EDLC, PAN fibers, Glycerol, KOH, Green electrolytes.

Posted Date: March 9th, 2023

DOI: https://doi.org/10.21203/rs.3.rs-2540617/v1

Version of Record: A version of this preprint was published at Waste and Biomass Valorization on July 4th, 2023. See the published version at https://doi.org/10.1007/s12649-023-02208-2.

Abstract

Amidst different types of energy storage systems, electric double-layer capacitors (EDLCs), also known as supercapacitors, have received considerable attention as energy storage alternatives due to their advantageous characteristics: high power density, long-life cycle, lightweight, safe operations, and fast charge-discharge rates. This work addresses these EDLC devices and has been divided into two parts. In the former, the synthesis and characterization of activated carbon fiber-felt (ACFF) electrodes from textile PAN fiber have been provided. In the latter, electrochemical characterization of the ACFF electrodes in potassium hydroxide solutions (aqueous-based) and in potassium hydroxide-glycerol hybrid electrolytes (glycerol-based electrolytes) have been investigated. The synthesis of ACFF electrodes via two-step oxidation, carbonization, and physical activation resulted in low-cost and binder-free electrodes containing mostly micropores (maximum pore width of 3 nm) and a specific surface area of 1875 $m^2 g^{-1}$. Electrochemical impedance spectroscopy, cyclic voltammetry, and galvanostatic charge-discharge techniques were carried out in a symmetric two-electrode setup at room temperature. The results showed that ACFF-based EDLCs in aqueous-based electrolyte (2 M KOH) exhibited low electrolyte resistance (0.44 ± 0.04 Ω cm^2) and high gravimetric capacitance (129 ± 6 F g^{-1} at 1 mV s^{-1}). Although ACFF-based EDLCs in glycerol-based electrolytes exhibited high electrolyte resistance (> 17 ± 2 Ω cm^2), they are hybrid green-electrolytes that support a large potential window (< 2.5), which is greater than that of aqueous electrolytes (≈ 1 V). Crude glycerol, the main byproduct in biodiesel production, is non-toxic, relatively safe, and low-cost. The advantages and disadvantages of aqueous and glycerol-based electrolytes have been discussed.

1. Introduction

Due to the growing demand for energy consumption and the development of new energy sources, energy storage devices are needed for balancing the energy supply and demand on the electrical grid system [1]. Among the different types of energy storage systems (ESS), supercapacitors (SCs), also known as electrochemical capacitors or ultracapacitors, have drawn the attention of the scientific community owing to their characteristics. The advantages of SCs are high power density, long-life cycle (> 100,000 cycles) [2], fast charge-discharge rates (from seconds to minutes), wide operating temperature range (-40°C to 70°C) [3], low maintenance, lightweight, and safe operations. According to the Ragone plot, supercapacitors bridge the gap between electrolytic capacitors and batteries. SCs have higher energy densities and can store more energy than electrostatic capacitors. In addition, SCs have higher power densities and can store and release energy faster than batteries [4]. Due to its high self-discharge rate, supercapacitors are not fitting for long-term energy storage [5]. In comparison to batteries, SCs have lower-energy storage capacity and are not well-suited for applications requiring high energy density [6]. Therefore, SCs can be used as a complement to other energy storage devices, such as batteries.

Based on the charge storage mechanism (faradaic and non-faradaic), supercapacitors are classified into three categories, namely electric double-layer capacitors (EDLC), pseudocapacitors, and hybrid

supercapacitors [7]. EDLCs store charge through physical adsorption-desorption of charged electrolyte ions at the surface of highly porous carbon-based electrodes; an electrostatic and non-faradaic mechanism [8]. Consequently, no charge transfer takes place between the electrolyte ions and the surface of the electrodes. Pseudocapacitors store charge through fast and reversible faradaic-redox reactions at the surface or near-surface of the electrode (a faradaic mechanism) [9]. Therefore, there is a transfer of charges at the electrode-electrolyte interfaces. Hybrid supercapacitors are based on two different mechanisms of charge storage: faradaic e non-faradaic. The negative electrode material, commonly a carbon-based electrode, is responsible for the power source and it stores charge non-faradaically [10]. Otherwise, the positive electrode material, commonly a metal oxide electrode, is responsible for the energy source and it stores charge faradaically [11].

EDLCs consist of two highly porous carbon-based electrodes (symmetric or asymmetric) in contact with an electrolyte solution, and a separator to isolate the two electrodes and prevent a short circuit [12]. As the electrochemical performance of supercapacitors strongly relies on the electrode-electrolyte interaction, correlating the size of electrolyte ions and the pore size of carbon-based electrodes is necessary. Electrodes and electrolytes are at the core of SCs research. Most research topics focus on electrode materials and only a few types of research focus on the study of electrolytes [13].

The electrochemical performance of electrodes depends on variables such as specific surface area (SSA), surface functional groups, and pore texture [14]. Due to high SSA, within a range of 1000–2500 $m^2\ g^{-1}$, activated carbons (ACs) are common examples of carbon-based electrodes for EDLCs [15]. Examples of ACs include granular activated carbon (GAC) and powder activated carbon (PAC). In AC-based electrodes, binders are utilized to provide strong adhesion between the electrode and the current collector. These binders cause pore blockage reducing the active surface area of the electrode, which impacts the electrochemical performance of the supercapacitor. Among the different types of activated materials, activated carbon fibers (ACF) can be converted into woven fabrics (yarn interlacing process), knit fabrics (yarn inter-looping process), or felt (matted non-woven fabric) offering them self-supporting characteristics. ACF-based electrodes, which are binder-free electrodes, have drawn attention not only because of high SSA (mostly micropores), but also due to a well-defined porous structure, and high adsorption capacity [16]. An example of a synthetic precursor used to produce ACFs is Polyacrylonitrile (PAN); a thermoplastic polymer with a high melting point of 350°C [17]. Textile PAN-based fibers are low-cost and alternative raw materials used to produce ACFs. In order to obtain self-supporting characteristics, textile PAN-based fibers are converted into a felt; a matted non-woven fabric [18].

Carbon-based electrodes in organic electrolytes such as acetonitrile (ACN) or propylene carbonate (PC) are commonly used for commercial supercapacitors [19]. Although organic-based electrolytes can support a large potential window (~ 3 V) [20], they are usually flammable and toxic [21]. Aqueous-based electrolytes are an alternative to organic-based electrolytes due to their advantages of high ionic conductivity (10^1 – 10^2 mS cm^{-1}) [22], non-flammability, low cost, low internal resistance, and low viscosity [23]. One of the drawbacks of aqueous-based electrolytes is the limited cell voltage (~ 1 V) due to their narrow

electrochemical stability window (ESW) [24]. The development of alternative electrolytes focuses on increasing the potential window (operating voltage) and consequently the energy density of the devices [25]. Previous studies proposed the use of glycerol as a deep eutectic solvent [26, 27]. Crude glycerol or 1,2,3-propanetriol ($C_3H_8O_3$), commonly called glycerin, is the main byproduct in biodiesel production. Glycerol is non-toxic, relatively safe, low-cost and a viscous green solvent with a high boiling point of 290°C and a low melting point of 18°C. Moreover, glycerol monomer has a hydroxyl-rich structure with three hydroxyl functional groups (alcohol group), also known as trihydric alcohol. The presence of hydroxyl groups (OH) increases ion mobility into the pores and enhances capacitance, which is the amount of charge stored [28].

This work addresses EDLC storage devices and it has been divided into two parts, namely: (1) synthesis and characterization of activated carbon fiber-felt electrodes from textile PAN-based fiber, and (2) electrochemical characterization of the electrodes in aqueous-based and glycerol-based electrolytes. The advantages and disadvantages of aqueous and glycerol-based electrolytes have also been discussed.

2. Experimental

2.1 Synthesis of activated carbon fiber-felt electrodes from textile PAN-based fiber

The synthesis of activated carbon fiber-felt (ACFF) electrodes was based on the methodology proposed in previous works [29, 30] and included three fundamental processes: oxidation, carbonization, and physical activation (Fig. 1).

A wet-spun tow of textile PAN-based fiber (5.0 dtex), with a bean-type cross-section, was supplied by JMHP and used as a raw material to produce the felt.

The fiber was transformed into a thermoset material through a two-step oxidation process, namely standard oxidation and over-oxidation. Standard oxidation was performed in two steps over 50 minutes: a pre-oxidation at 245°C and subsequent oxidation at 250°C. According to the proposed methodology, oxidation time affects the surface chemistry of carbon-based materials and leads to the development of nitrogen groups. These nitrogen compounds, particularly the pyrrolic and the pyridinic functional groups, contribute to increased capacitance. Over-oxidation was carried out for 90 min at 250° C: totaling 140 min for the entire oxidation process.

Oxidized textile PAN fiber was converted into a felt (200 g m^{-2}) through a standard needle felting process (non-woven) and designated as oxidized textile-Pan fiber-felt (OPFF).

OPFF underwent carbonization and physical activation processes. Both processes were carried out in a horizontal tube furnace.

The OPFF sample, with a size of 0.32 m^2, a weight of 50 g, and 3 mm in thickness, was cut and placed in an appropriate sample holder. The carbonization of the OPFF sample was carried out under an inert atmosphere. The sample was heated from room temperature to 900°C at a heating rate of 30°C min^{-1} and 20 min of residence time. Subsequent carbonization and prior physical activation, the argon gas flow was switched off and replaced with carbon dioxide (200 sccm). A syringe was used to introduce a total of 12 ml of water during steam activation. Physical activation was carried out under an oxidizing atmosphere at 1000°C and 60 min of residence time.

Subsequent physical activation, the gas flow was switched off and replaced with argon, and the furnace was turned off. The inert atmosphere was kept through the cooling process until room temperature. The activated carbon fiber-felt sample was designated as ACFF.

2.2 Textural and structural characterization of ACFF electrodes

Textural and structural characterizations of the electrodes were carried out prior to the electrochemical characterizations.

Brunauer–Emmett–Teller (BET) equation and density functional theory (DFT) method were applied to analyze the surface area and the pore size distribution of ACFF samples, respectively. Nitrogen (N_2) adsorption–desorption isotherms at 77 K were measured using an ASAP 2020 Plus adsorption analyzer by Micromeritics. Prior to the measurements, degasification of the sample was performed at 120°C for 12 h under vacuum pressure of 5 μmHg.

The structural characterization of ACFF samples was carried out by Raman-scattering spectroscopy technique using Horiba Scientific model Labram HR Evolution. Ar ion laser operating at 512 nm and scan mode of 1000–2500 cm^{-1} were employed to collect Raman spectra.

2.3 Electrolyte selection

In order to understand the electrochemical behavior of the ACFF electrodes in aqueous-based and glycerol-based electrolytes, the selection of said electrolytes was based on a previous work [31] about supercapacitors prepared with electrolytes of low environmental impact. As an example of a conventional and strong alkaline electrolyte, potassium hydroxide (KOH) solutions with molar concentrations of 1 mol L^{-1} and 2 mol L^{-1} were used as aqueous-based electrolytes. Aiming to investigate green electrolytes, potassium hydroxide-glycerol hybrid electrolytes (KOH:GLY) with molar ratios of 1:1, 2:1, and 3:1 were used as glycerol-based electrolytes.

2.4 Assembly of the EDLC cell

The ACFF sample was cut into small disks with a diameter of 8 mm and a cross-sectional area of 0.5 cm^{-2}. In order to remove moisture, the ACFF electrodes underwent a drying process for 2 hours at 110°C. Subsequent drying, the electrodes were weighted and stored in a round vacuum desiccator. The active

mass and the active mass loading of each ACFF electrode are 3.6 ± 0.1 mg and 1.8 ± 0.1 mg cm^{-2}, respectively.

Before assembling the symmetric EDLC cell, moisture-free ACFF electrodes were immersed in aqueous-based electrolyte for 24 hours (Fig. 2a). Due to the high viscosity of glycerol-based electrolytes and in order to improve electrolyte diffusion, electrode-electrolyte contact for approximately 2 hours, at room temperature, is recommended (Fig. 2b). Subsequent to electrolyte diffusion, KOH:GLY samples were stored in vacuum desiccators for 48 hours to remove moisture (Fig. 2c).

A qualitative filter paper (0.2 mm in thickness) was cut into small disks with a diameter of 10 mm and used as a separator to keep the two electrodes apart and prevent a short circuit (Fig. 2d). Symmetric EDLC was assembled in a two-electrode Swagelok®-cell with a Teflon case and two graphite rods as current collectors (Fig. 2e).

2.5 Electrochemical characterization

Electrochemical impedance spectroscopy (EIS), cyclic voltammetry (CV), and galvanostatic charge-discharge (GCD) techniques were conducted to evaluate the performance and the electrochemical characteristics of ACFF electrodes in aqueous-based and glycerol-based electrolytes. All electrochemical measurements were carried out in a symmetric two-electrode configuration cell (Swagelok®-type) at room temperature in a multichannel potentiostat Parstat MC by Princeton Applied Research. Origin version 9.70 was used for data analysis and graphing.

Cyclic voltammetry was used to determine the specific capacitance, also known as gravimetric capacitance, of the EDLC devices. Capacitance (C), which is the ability to store charge per volt, is given in units of Farads (F) [32]. As capacitance is inversely proportional to the distance between the electrodes and directly proportional to their surface area, electrodes with a high surface area lead to an increase in capacitance and, as a result, higher energy density [33]. The value of gravimetric capacitance (C_s) was calculated from the integration of the area under the CV curve according to Eq. 13 [34]:

$$C_{s(CV)} = \frac{\left(\frac{\int_{ui}^{uf} i(U)d(U)}{2v(Uf-Ui)}\right)4}{(m_1+m_2)}$$

1

where C_s is given in units of Farads per gram (F g^{-1}), $\int_{ui}^{uf} i\,(U)\,d\,(U)$ is the area under the curve (V A), v is the scan rate (V s^{-1}), $m_1 + m_2$ is the active mass of both electrodes (g), and $Uf - Ui$ is the potential difference (V). The percentage error of specific capacitance value was 5%.

CV measurements were conducted at a scan rate of 1 mV s^{-1} for both aqueous-based and glycerol-based electrolytes. Due to water electrolysis (decomposition at 1.23 V) [35], CV measurements of aqueous-based

electrolytes were carried out within a potential window of 0–1 V. Due to the wide electrochemical stability window (ESW), the measurements of glycerol-based electrolytes were carried out within a potential window of 0–2.1 V.

GCD and EIS experiments for aqueous-based and glycerol-based electrolytes were carried out at the same condition.

Galvanostatic charge-discharge was used to determine the equivalent series resistance (ESR) of the EDLC devices. As the voltage drop (IR_{drop}) is related to the internal resistance of the cell when the current is interrupted or inversed, the value of equivalent series resistance (ESR) was deduced according to Eq. 2 [36]:

$$ESR = \left| \frac{IR_{drop}}{2I} \right|$$

2

where ESR is given in units of Ohms (Ω), I is the applied current (A), and IR_{drop} is the voltage drop (V). The percentage error of ESR value was 10%. GCD measurements were conducted at a potential window of 0–1 V and a current density of 0.15 A g^{-1}.

Electrochemical impedance spectroscopy, a frequency response technique, was applied to analyze the interaction at the electrode-electrolyte interface. EIS measurements were performed with a frequency range of 10^{-3} Hz – 10^{6} Hz, applied signal amplitude of 5 mV, applied potential of 0V, and it was expressed graphically in a Nyquist plot.

The value of gravimetric energy density (E_s), which is the amount of energy stored per unit of volume or weight [37], was calculated according to Eq. 3 [38]:

$$E_s = \frac{1}{2} C_s V^2 \frac{1}{3.6}$$

3

where E_s is given in units of watt-hours per kilogram (Wh kg^{-1}), C_s is the gravimetric capacitance (F g^{-1}), and V is the maximum voltage (V). The percentage error of gravimetric energy density value was 5%.

The value of specific power (P_s), which is the maximum power output per unit of mass, depends on the voltage and on the internal resistance of the cell (ESR). P_s was calculated according to Eq. 4 [39]:

$$P_s = \frac{V}{4Rm}^2$$

4

where P_s is given in units of watt per kilogram (W kg^{-1}), R is the internal resistance of the cell (Ω), m is the total electrode mass (kg), and V is the applied voltage (V). The percentage error of specific power value was 5%.

3. Results And Discussion

3.1 Synthesis of ACFF electrodes from textile PAN-based fiber

The purpose of thermal-oxidative stabilization, also known as oxidation, is to provide a structure that can withstand high temperatures and to prevent degradation and melting of the fiber in the subsequent carbonization process. Thermoplastic textile PAN-based fibers are converted into thermosetting fibers due to the cyclization of nitrile groups and the cross-linking of PAN chains [40]. Once stabilized, the PAN-based sample containing carbon and noncarbon elements, such as nitrogen, hydrogen, and oxygen, undergoes a carbonization process. As a result, noncarbon elements are removed and released as volatile gases resulting in weight loss and shrinkage of the sample [41].

Activation is the key process in the synthesis of carbon-based electrodes due to the development of accessible porosity that leads to an improved surface area. During the activation process, existing clogged pores that were developed during carbonization are opened up and enlarged. In addition, new porosity is developed resulting in a well-defined porous structure and an enhanced surface area [42]. Physical activation is an uncomplicated and effective process, although it requires high temperatures (700–1200°C) and some of the carbon atoms are removed during the process resulting in low production yield [43]. The most common examples of oxidizing agents are O_2, CO_2, and steam. Previous studies reported that CO_2 leads to a higher development of narrow microporosity, and hence it was chosen as the major oxidizing agent [44]. As a combination of two oxidizing agents contributes to the development of enhanced porosity, water (steam) was chosen as the minor oxidizing agent. While CO_2 leads to the development of new microporosity, water helps to widen the existing micropores. Since water requires lower temperatures in comparison to CO_2, water was used in the first stage of the activation process. If the activation time is overextended, the development of mesopores (< 2 - > 50 nm) occurs by burning off the wall bordering the micropores (> 2 nm) [45]. Subsequent to the carbonization-activation process, the ACFF sample had a burn-off of 21%, a total mass loss of 79%, and a shrank of 55% in size.

3.2 Characterization of the ACFF electrodes

According to the IUPAC classification of adsorption Isotherms for gas-solid equilibria [46], the N_2 adsorption-desorption isotherm of ACFF electrodes, shown in Fig. 3a, is classified as Type I and indicates a microporous character. Moreover, hysteresis is absent, which suggests that the size of the pores measured on adsorption and desorption branches coincides well. [47]. BET theory was applied to calculate

the specific surface area (S_{BET}) of ACFF electrodes from the acquired data of N_2 adsorption at 77 K. In accordance with the results, ACFF electrodes have a high S_{BET} value of 1875 $m^2 g^{-1}$ and a correlation coefficient (r) of 0.999918. The microporosity developed particularly during the activation process contributed to the high value of the specific surface area.

The mobility of the ions into the pores depends on the pore size. Thus, inaccessible pores do not contribute to both double-layer capacitance and energy density [48]. Previous studies suggested that pore size smaller than 0.5 nm is inaccessible to hydrated ions [49]. The technique applied for pore size distribution (Fig. 3b) does not show any information about pores smaller than 1 nm due to the penetration limit of N_2. Regardless of the limitation, an ascending line in the region of pore width smaller than 1 nm possibly indicates the presence of said micropores [50]. The pore size distribution curve determined by the DFT method shows a maximum pore width of 3 nm. Furthermore, the size of most pores ranges from 1 to 2 nm confirming the presence of microporosity. As reported in the literature, a small number of pores, wider than 2 nm, increase the power density of SCs [51]. These small mesopores facilitate the access of electrolyte ions into the electrode surface. The average pore size of PAN-based ACF reported in the literature ranges from 4 to 10 nm [52]. The average pore size of the ACFF sample is smaller due to the parameters of the activation process. The development of porosity is influenced by several factors such as the residence time, temperature, original porosity and structure of the carbonized material, pressure and flow rate of the gas, and the type of oxidizing agent [53].

The Raman spectrum for carbon-based materials, amorphous or crystalline, exhibits two well-defined peaks commonly assigned as D and G bands. The D band, also known as the disorder/defect band, exhibits a peak at nearly 1380 cm^{-1}. The G band, crystalline graphite, exhibits a peak at nearly 1580 cm^{-1} due to the C-C bond-stretching of all pairs of sp^2 atoms in both rings and chains [54].

The Raman spectra of ACFF electrodes are shown in Fig. 4. In all samples, the spectra exhibited the same appearance. There are two very broad peaks located in the range of 1244–1710 cm^{-1}. The first peak, located at 1342 cm^{-1}, is referred to “D”. The second peak, located at 1598 cm^{-1} is referred to “G”. The spectra of ACFF electrodes are very similar to that of carbon-based materials.

3.3 Electrochemical performance

Figure 5 shows a comparison of the CV curves measured for aqueous-based and glycerol-based electrolytes at a scan rate of 1m V s^{-1}. As capacitance is constant over an acknowledged potential window, symmetric and nearly rectangular curves in the cyclic voltammograms are expected for carbon-based EDLC devices [55]. Therefore, in comparison to glycerol-based electrolytes, aqueous-based electrolytes exhibited less distorted rectangular-shaped curves that indicate mostly electrostatic capacitance (a non-faradaic mechanism), good reversibility and low resistance. Furthermore, glycerol-based electrolytes, particularly molar ratios of 1:1 and 2:1, exhibited blunt CV profiles indicating the possibility of higher values for equivalent series resistances (ESR) [56]. The tail observed in the CV curves

of KOH:GLY possibly indicates the presence of water content due to the fact that both components of the glycerol-based electrolyte are hygroscopic. Moreover, the tail observed in the CV curves of aqueous-based electrolytes suggests electrochemical decomposition of the electrolyte at high potentials due to water electrolysis [57]. The narrow potential window of aqueous-based electrolyte limits energy density and restricts the amount of energy stored [58].

Among the ACFF-based EDLCs, aqueous KOH electrolyte at a molar concentration of 2 mol L^{-1} exhibited the highest gravimetric capacitance value of 129 ± 6 F g^{-1} at a scan rate of 1 mV s^{-1}. Amidst glycerol-based electrolytes, KOH:GLY (2:1) exhibited the highest gravimetric capacitance value of 99 ± 5 F g^{-1} possibly due to the long tail, which could affect overall electrochemical performance. KOH:GLY (3:1) exhibits less distorted rectangular-shaped curves and a much shorter tail, which suggest an improved performance and lower resistance.

The absence of humps or redox peaks in the CV curves of ACFF-based EDLCs suggests that there is no occurrence of oxidation-reduction reactions, which is expected from an electrostatic and non-faradaic mechanism [59]. Nevertheless, previous literature reported that carbon-based electrodes possibly exhibit 1–5% of their capacitance as surface-redox pseudocapacitance due to reversible faradaic-redox reactions of active surface functional groups [60]. As explained previously, oxidation time affects the surface chemistry of AC-based materials leading to enhanced capacitance. The occurrence of a minor surface-redox pseudocapacitive behavior could be verified with a three-electrode cell at a low scan rate instead of a two-electrode cell.

Figure 6 shows the Nyquist plot for aqueous-based and glycerol-based electrolytes at an applied potential of 0 V; where $-Z_{im}$ is the imaginary part (capacitive) and Z_{re} is the real part (resistive) [61]. A Nyquist plot exhibits three distinct frequency regions: (1) a high-frequency region that is higher than 10 kHz (low values for Z_{re}), (2) a medium-frequency region, ranging from 10 kHz to 1 Hz, and (3) a low-frequency region that is lower than 1 Hz (high values for Z_{re}) [62].
At high frequencies, the behavior of a supercapacitor is comparable to a resistance and it is related to the bulk solution resistance of the electrolyte [63]. The value of electrolyte resistance (R_s) can be deduced at the point where the plot intercepts the x-axis of the Nyquist plot, also known as the real axis (Z_{re}) [64]. The results are normalized by Ω cm^{-2} for comparison.

Aqueous-based electrolytes have low electrolyte resistance in comparison to glycerol-based electrolytes. The lowest value of R_s (0.44 ± 0.04 Ω cm^2) can be observed in aqueous KOH electrolyte, at a molar concentration of 2 mol L^{-1} (Fig. 6a). Among glycerol-based electrolytes (Fig. 6b), KOH: GLY (3:1) exhibited the lowest value of Rs (17 ± 2 Ω cm^2) probably due to the salt concentration as conductivity can be affected by the salt-to-solvent ratio [65].

The interfacial impedance between the bulk solution (electrolyte) and the electrode can be observed at medium frequencies. A conventional Nyquist plot for an EDLC cell exhibits a single semicircle that

represents the ion charge-transfer resistance (R_{ct}), and its diameter is related to the ion mobility in the pores [66]. A single semicircle can be seen in both concentrations of aqueous-based electrolytes. The values of R_{ct} for aqueous KOH electrolyte, at a molar concentration of 1 and 2 mol L^{-1} are 0.59 ± 0.06 Ω (0.30 ± 0.03 Ω cm^2) and 0.36 ± 0.04 Ω (0.18 ± 0.18 Ω cm^2), respectively. The absence of a single semicircle in glycerol-based electrolytes may occur due to the minimal impedance of the electrolyte [67].

Subsequent to the semicircle, a 45-degree line, or slope, at the low frequency region indicates ion diffusion within the pores [68]. While 2 M KOH exhibits a steep slope after the semicircle, 1 M KOH and KOH:GLY (3:1) exhibit gradual slopes. A steep slope suggests that ion penetration into pores occurs efficiently. A gradual slope, as in the case of 1 M KOH and KOH:GLY (3:1), suggests that ion penetration into pores occurs laboriously [69].

A vertical line at the low-frequency region parallel to the imaginary part (y-axis) is expected for an ideal capacitor [70]. The 90-degree line, or tail, suggests that capacitance is constant over the applied frequency range and the electrode surface is entirely impregnated [71], A vertical line can be observed in the Nyquist plot for both concentrations of aqueous-based electrolytes (Fig. 6a), and nearly vertical line can be observed in the glycerol-based electrolyte KOH:GLY (3:1) (Fig. 6b). The Nyquist plots of KOH:GLY with molar ratios of 1:1 and 2:1 deviate from the profile expected from an ideal EDLC. The line (tail) of 2 M KOH leans more towards the $-Z_{im}$ axis (y-axis), which is the imaginary part (capacitive) of the Nyquist plot, indicating that the ACFF-based EDLC in aqueous 2 M KOH has a better capacitive behavior.

While R_s and R_{ct} rely upon the electrolyte solution, the tail depends on both electrode and electrolyte. Due to the low viscosity of its solvent, aqueous-based electrolytes (Fig. 2a) have high ionic conductivity (10^1 – 10^2 mS cm^{-1}) [72] which improves ion mobility and results in smaller values for R_s and R_{ct} [73]. On the contrary, glycerol-based electrolytes (Fig. 2b) have high viscosity and do not provide good contact in the electrode-electrolyte interface. As ion mobility is inversely proportional to the size of the ion, large molecules, such as glycerol molecules, have high resistivity. Thus, large pores in the surface of the electrode are required since inaccessible pores do not contribute to the double layer capacitance [74].

The results are in agreement with the cyclic voltammogram data discussed in the preceding section. Aqueous-based electrolytes exhibited higher values for gravimetric capacitance and nearly CV rectangular-shaped curves indicating lower resistance and better electrochemical performance.

Near-isosceles triangular-shaped curves are expected for carbon-based EDLC devices and suggest primarily an electrostatic (non-faradaic) mechanism [75]. Among the ACFF-based EDLCs, aqueous KOH electrolyte at a molar concentration of 2 mol L^{-1} (Fig. 7a) exhibited near-isosceles triangular-shaped curves. Aqueous KOH electrolyte at a molar concentration of 1 mol L^{-1} (Fig. 7b) also exhibits triangular-shaped curves, although the nonlinear charging curve reaching a plateau at high potentials may indicate decomposition of the electrolyte possibly due to overcharge [76]. Among the glycerol-based electrolytes,

only KOH:GLY with a molar ratio of 3:1 exhibited triangular-shaped curves (Fig. 7d). The discharge curves of both aqueous-based electrolytes and KOH:GLY (3:1) drop linearly indicating that there is no considerable contribution of pseudocapacitance because the charge storage mechanism is manly electrostatically [77]. The GCD curves of KOH:GLY with molar ratios of 1:1 and 2:1 do not drop linearly and deviate from the profile expected from an ideal EDLC (Fig. 7e – 7f).
The equivalent series resistance of the cell (ESR), also known as internal resistance, consists of the bulk solution resistance of the electrolyte (R_s), the electrode-electrolyte interfacial resistance (R_{ct}), the resistance of intra-particle pores, and the contact resistance between the current collector and the electrode [78]. For a better electrochemical performance, a low ESR value is preferred.

Voltage drop (IR-drop), which is the resistance of the cell, was used to deduce the value of ESR. At a current density of 0.15 A g^{-1}, the occurrence of IR-drop is noticeable in all glycerol-based electrolytes (Fig. 7d-7f). Among all glycerol-based electrolytes, KOH: GLY (3:1) exhibited the lowest value for ESR (Table 1) apparently due to the salt concentration as electrolyte conductivity can be affected by the salt-to-solvent ratio.

Table 1
Value of ESR in glycerol-based electrolytes at a current density of 0.15 A g^{-1}

		ESR (Ω)	ESR (Ω cm^2)
Glycerol-based	KOH:GLY (3:1)	76 ± 4	38 ± 2
	KOH:GLY (2:1)	193 ± 10	97 ± 5
	KOH:GLY (1:1)	390 ± 20	195 ± 10

The occurrence of IR-drop in aqueous-based electrolytes is not noticeable in small current densities, such as 0.15 A g^{-1}. Due to the nature of aqueous-based electrolytes (high conductivity and low viscosity) larger current densities were required. The occurrence of IR-drop in aqueous 2 M KOH is only noticeable at current densities ≥ 8 A g^{-1} (Fig. 8A). Even in larger current densities, aqueous 2 M KOH exhibits triangular-shaped curves, a discharge curve that drops linearly, and low internal resistance (0.83 ± 0.04 Ω cm^2) indicating satisfactory electrochemical performance. Although aqueous 1 M KOH performed better than glycerol-based electrolytes, the occurrence of IR-drop is noticeable at current densities > 1 A g^{-1} (Fig. 8b); an inferior performance in comparison to 2 M KOH.
The results are in agreement with the Nyquist plot discussed in the preceding section. Aqueous-based electrolytes have high ionic conductivity and wettability which enhance electrode-electrolyte interaction and consequently decrease ESR values.

Table 2
Gravimetric energy density (E_s) and specific power (P_s) of ACFF-based EDLCs

Type of electrolyte		E_s (Wh kg^{-1})	P_s (kW kg^{-1})
Aqueous-based	1 M KOH	14 ± 1	3.5 ± 0.3
	2 M KOH	18 ± 1	17.9 ± 1.8
Glycerol-based	KOH:GLY (1:1)	48 ± 2	0.1 ± 0.1
	KOH:GLY (2:1)	61 ± 3	0.2 ± 0.1
	KOH:GLY (3:1)	50 ± 3	0.4 ± 0.1

Previous literature reported that the gravimetric energy density, also known as specific energy, for EDLCs commonly ranges from 5–10 Wh Kg^{-1} [79]. As can be seen in Table 2, the energy density of all ACFF-based EDLCs exhibited superior performance. According to Eq. 3, gravimetric energy density is proportional to gravimetric capacitance (C_s) and the square of the voltage (V). As a result, increasing either or both of them enhances the energy density of EDLCs and expands the range of SCs applications. Although aqueous-based electrolytes exhibited higher values for gravimetric capacitance (Fig. 5), glycerol-based electrolytes exhibited higher values for energy density due to the electrochemical stability window of the hybrid electrolyte, which is twice greater.

ESR limits power density and the energy cannot be delivered completely due to the distance between the electrolyte and the electrode [80]. As can be seen in Table 2, aqueous-based electrolytes exhibited higher values of specific power (P_s) in comparison to glycerol-based electrolytes due to low internal resistance. In order to improve the specific power of glycerol-based electrolytes, decreasing the values of ESR and improving the ionic conductivity is suggested.

4. Conclusions

The synthesis of activated carbon fiber-felt electrodes (ACFF) via two-step oxidation, carbonization, and physical activation processes resulted in low-cost, binder-free and highly porous carbon-based electrodes with a specific surface area of 1875 m^2 g^{-1}, maximum pore width of 3 nm, and the size of most pores ranging from 1 to 2 nm. ACFF-based EDLCs exhibit satisfactory electrochemical performance in aqueous-based electrolytes resulting in a gravimetric capacitance value of 129 ± 6 F g^{-1} at 1 mV s^{-1}, low internal resistance (0.83 ± 0.04 Ω cm^2 at 8 A g^{-1}), and low electrolyte resistance (0.44 ± 0.04 Ω cm^2). Although aqueous-based electrolytes have high conductivity and low viscosity, the cell voltage is limited (~ 1 V) due to the narrow electrochemical stability window.

ACFF-based EDLCs in glycerol-based electrolyte, KOH:GLY with a molar ratio of 3:1, exhibited a gravimetric capacitance of 82 ± 4 F g^{-1} at 1 mV s^{-1}, high internal resistance (38 ± 2 Ω cm^2 at 0.15 A g^{-1}) and high electrolyte resistance (17 ± 2 Ω cm^2). Although high resistance and high viscosity are drawbacks in electrochemical performance, glycerol-based electrolyte (KOH:GLY 3:1) is a low-cost, non-toxic and heat-resistant hybrid green-electrolyte that supports a large potential window (< 2.5).

The electrochemical performance of supercapacitors strongly relies on the electrode-electrolyte interaction and correlating the size of electrolyte ions and the pore size of carbon-based electrodes is necessary. Glycerol-based electrolytes have large molecules that are not well-fitting for the pore width of the ACFF electrode synthesized in this work. Inaccessible pores do not contribute to double-layer capacitance, and it is suggested to change the parameters of the physical activation process. The viscosity of the electrolyte and consequently ion mobility and ion diffusion could be improved by heating.

Declarations

Funding

This work was supported by the Academic Excellence Program (PROEX) within the Coordination for the Improvement of Higher Education Personnel (CAPES). Textile Pan-based fiber was supplied by JMHP Carbon.

Competing Interests

The authors have no competing interests to declare that are relevant to the content of this article.

Author Contributions

All authors contributed to the study conception and design. Material preparation, data collection and analysis were performed by Ingrid Ariani Belineli, Jossano Saldanha Marcuzzo, Ivana Conte Cosentino and Rubens Nunes de Faria Junior. The first draft of the manuscript was written by Ingrid Ariani Belineli Barbosa and all authors commented on previous versions of the manuscript. All authors read and approved the final manuscript.

Data availability

The datasets generated during and/or analyzed during the current study are available from the corresponding author on reasonable request.

References

1. Arbizzani, C., Yu, Y., Li, J., Xiao, J., Xia, Y., Yang, Y., et al.: Good practice guide for papers on supercapacitors and related hybrid capacitors for the Journal of Power Sources. J. Power Sources. **450**, 227636 (2020 Feb)
2. Pal, B., Yang, S., Ramesh, S., Thangadurai, V., Jose, R.: Electrolyte selection for supercapacitive devices: a critical review. Nanoscale Adv. **1**(10), 3807–3835 (2019)
3. Yang, Y., Han, Y., Jiang, W., Zhang, Y., Xu, Y., Ahmed, A.M.: Application of the Supercapacitor for Energy Storage in China: Role and Strategy. Applied Sciences. 2021 Dec 30;12(1):354
4. Yadlapalli, R.T., Alla, R.R., Kandipati, R., Kotapati, A.: Super capacitors for energy storage: Progress, applications and challenges. J. Energy Storage. **49**, 104194 (2022 May)
5. Olabi, A.G., Abbas, Q., Al Makky, A., Abdelkareem, M.A.: Supercapacitors as next generation energy storage devices: Properties and applications. Energy. **248**, 123617 (2022 Jun)
6. González, A., Goikolea, E., Barrena, J.A., Mysyk, R.: Review on supercapacitors: Technologies and materials. Renewable and Sustainable Energy Reviews [Internet]. Available from: (2016). May;58:1189–206 https://www.sciencedirect.com/science/article/pii/S1364032115016329
7. Pore, O.C., Fulari, A.V., Shejwal, R.V., Fulari, V.J., Lohar, G.M.: Review on recent progress in hydrothermally synthesized MCo2O4/rGO composite for energy storage devices. Chem. Eng. J. **426**, 131544 (2021 Dec)
8. Barzegar, F., Momodu, D.Y., Fashedemi, O.O., Bello, A., Dangbegnon, J.K., Manyala, N.: Investigation of different aqueous electrolytes on the electrochemical performance of activated carbon-based supercapacitors. RSC Adv. **5**(130), 107482–107487 (2015)
9. Brousse, T., Bélanger, D., Long, J.W.: To Be or Not To Be Pseudocapacitive? J. Electrochem. Soc. **162**(5), A5185–A5189 (2015)
10. Yang, Y., Han, Y., Jiang, W., Zhang, Y., Xu, Y., Ahmed, A.M.: Application of the Supercapacitor for Energy Storage in China: Role and Strategy. Applied Sciences. 2021 Dec 30;12(1):354
11. Olabi, A.G., Abbas, Q., Al Makky, A., Abdelkareem, M.A.: Supercapacitors as next generation energy storage devices: Properties and applications. Energy. **248**, 123617 (2022 Jun)
12. Winter, M., Brodd, R.J.: What Are Batteries, Fuel Cells, and Supercapacitors? Chemical Reviews. ;104(10):4245–70. (2004) Oct
13. Bhat, T.S., Patil, P.S., Rakhi, R.B.: Recent trends in electrolytes for supercapacitors. J. Energy Storage. **50**, 104222 (2022 Jun)
14. Sagadevan, S., Marlinda, A.R., Chowdhury, Z.Z., Wahab, Y.B.A., Hamizi, N.A., Shahid, M.M., et al.: Fundamental electrochemical energy storage systems.Advances in Supercapacitor and Supercapattery. ;27–43. (2021)
15. Aziz, S.B., Hamsan, M.H., Brza, M.A., Kadir, M.F.Z., Muzakir, S.K., Abdulwahid, R.T.: Effect of glycerol on EDLC characteristics of chitosan:methylcellulose polymer blend electrolytes. J. Mater. Res. Technol. **9**(4), 8355–8366 (2020 Jul)

16. Chen, J.Y.: 1 - Introduction [Internet]. Chen JY, editor. ScienceDirect. Oxford: Woodhead Publishing; [cited 2022 Dec 14]. p. 3–20. Available from: (2017). https://www.sciencedirect.com/science/article/pii/B9780081006603000018)
17. Yue, Z., Economy, J.: 4 - Carbonization and activation for production of activated carbon fibers [Internet]. Chen JY, editor. ScienceDirect. Oxford: Woodhead Publishing; [cited 2022 Dec 16]. p. 61–139. Available from: (2017). https://www.sciencedirect.com/science/article/pii/B9780081006603000043)
18. Marcozzu, J.S., Cuña, A., Tancredi, N., Mendez, E., Bernardi, H.H.: Microporous activated carbon fiber felt from Brazilian textile PAN fiber: preparation, characterization and application as super capacitor electrode. Revista Brasileira de Aplicações no Vácuo. **35**, 38 (2016)
19. Barzegar, F., Momodu, D.Y., Fashedemi, O.O., Bello, A., Dangbegnon, J.K., Manyala, N.: Investigation of different aqueous electrolytes on the electrochemical performance of activated carbon-based supercapacitors. RSC Adv. **5**(130), 107482–107487 (2015)
20. González, A., Goikolea, E., Barrena, J.A., Mysyk, R.: Review on supercapacitors: Technologies and materials. Renewable and Sustainable Energy Reviews [Internet]. Available from: (2016). May;58:1189–206 https://www.sciencedirect.com/science/article/pii/S1364032115016329
21. Taer, E., Febriyanti, F., Apriwandi, Taslim, R., Agustino, Sinta Mustika, W.: Investigation of H_2SO_4 and KOH aqueous electrolytes on the electrochemical performance of activated carbon derived from areca catechu husk. Journal of Physics: Conference Series. Jun 1;1940(1):012033. (2021)
22. Chen, J., Lee, P.S.: Electrochemical Supercapacitors: From Mechanism Understanding to Multifunctional Applications. Advanced Energy Materials. Dec 21;11(6):2003311. (2020)
23. Bhat, T.S., Patil, P.S., Rakhi, R.B.: Recent trends in electrolytes for supercapacitors. J. Energy Storage. **50**, 104222 (2022 Jun)
24. Scibioh, M.A., Viswanathan, B.: Electrolyte materials for supercapacitors.Materials for Supercapacitor Applications. ;205–314. (2020)
25. Rodrigues, A.C., da Silva, E.L., Quirino, S.F., Cuña, A., Marcuzzo, J.S., Matsushima, J.T., et al.: Ag@Activated Carbon Felt Composite as Electrode for Supercapacitors and a Study of Three Different Aqueous Electrolytes. Materials Research. Nov 8;22(1). (2018)
26. Cojocaru, A., Brincoveanu, O., Pantazi, A., Balan, D., Enachescu, M., Visan, T., et al.: Electrochemical preparation of Ag nanoparticles involving choline chloride - glycerol deep eutectic solvents. Bulgarian Chemical Communications [Internet]. [cited 2022 Dec 16];49:194–204. Available from: (2017). http://www.bcc.bas.bg/BCC_Volumes/Volume_49_Special_C_2017/BCC22_49-C-2017_Anicai_p194.pdf
27. Lenardão, E.J., Manke Barcellos, A., Penteado, F., Alves, D., Perin, G.: Glycerol as a Solvent in Organic Synthesis. Revista Virtual de Química [Internet]. 2017 [cited 2022 Dec 16];9(1):192–237. Available from: http://static.sites.sbq.org.br/rvq.sbq.org.br/pdf/v9n1a15.pdf
28. Aziz, S.B., Hamsan, M.H., Brza, M.A., Kadir, M.F.Z., Muzakir, S.K., Abdulwahid, R.T.: Effect of glycerol on EDLC characteristics of chitosan:methylcellulose polymer blend electrolytes. J. Mater. Res.

Technol. **9**(4), 8355–8366 (2020 Jul)

29. Rodrigues, A.C., Munhoz, M.G.C., Pinheiro, B.S., Batista, A.F., Amaral-Labat, G.A., Cuña, A., et al.: N-activated carbon fiber produced by oxidation process design and its application as supercapacitor electrode.Journal of Porous Materials. 2019 Aug28;27(1):141–9
30. Marcozzu, J.S., Cuña, A., Tancredi, N., Mendez, E., Bernardi, H.H.: Microporous activated carbon fiber felt from Brazilian textile PAN fiber: preparation, characterization and application as super capacitor electrode. Revista Brasileira de Aplicações no Vácuo. **35**, 38 (2016)
31. Tatei, T.Y.: Estudo das características eletroquímicas de supercapacitores preparados com eletrólitos à base de líquido iônico (LIs) de baixo impacto ambiental
32. Winter, M., Brodd, R.J.: What Are Batteries, Fuel Cells, and Supercapacitors? Chemical Reviews. ;104(10):4245–70. (2004) Oct
33. Olabi, A.G., Abbas, Q., Al Makky, A., Abdelkareem, M.A.: Supercapacitors as next generation energy storage devices: Properties and applications. Energy. **248**, 123617 (2022 Jun)
34. Faria Junior, R.N.: de. 5.1. MEDIDAS Elétricas: Avaliação da capacitância por voltametria cíclica. In: Supercapacitor: conceitos básicos, materiais e métodos. São Paulo: Ed. Dos Autores; p. 117–127. (2021)
35. Brousse, T., Bélanger, D., Long, J.W.: To Be or Not To Be Pseudocapacitive? J. Electrochem. Soc. **162**(5), A5185–A5189 (2015)
36. de Faria Junior, R.N.: 5.4. MEDIDAS Elétricas: Avaliação da ESR pelo método automático da variação instantânea do potencial elétrico usando um galvanostato. In: Supercapacitor: conceitos básicos, materiais e métodos, pp. 138–144. Ed. Dos Autores, São Paulo (2021)
37. Scibioh, M.A., Viswanathan, B.: Characterization methods for supercapacitors.Materials for Supercapacitor Applications. ;315–72. (2020)
38. Rodrigues, A.C., da Silva, E.L., Quirino, S.F., Cuña, A., Marcuzzo, J.S., Matsushima, J.T., et al.: Ag@Activated Carbon Felt Composite as Electrode for Supercapacitors and a Study of Three Different Aqueous Electrolytes. Materials Research. Nov 8;22(1). (2018)
39. González, A., Goikolea, E., Barrena, J.A., Mysyk, R.: Review on supercapacitors: Technologies and materials. Renewable and Sustainable Energy Reviews [Internet]. Available from: (2016). May;58:1189–206 https://www.sciencedirect.com/science/article/pii/S1364032115016329
40. Jiménez, V., Sánchez, P., Romero, A.: 2 - Materials for activated carbon fiber synthesis [Internet]. Chen JY, editor. ScienceDirect. Oxford: Woodhead Publishing; [cited 2022 Dec 16]. p. 21–38. Available from: (2017). https://www.sciencedirect.com/science/article/pii/B978008100660300002X
41. Zhang, X.H., Li, Q.W.: 3 - Carbon fiber spinning [Internet]. Chen JY, editor. ScienceDirect. Oxford: Woodhead Publishing; p. 39–60. Available from: (2017). https://www.sciencedirect.com/science/article/pii/B9780081006603000031
42. Taer, E., Febriyanti, F., Apriwandi, Taslim, R., Agustino, Sinta Mustika, W.: Investigation of H_2SO_4 and KOH aqueous electrolytes on the electrochemical performance of activated carbon derived from

areca catechu husk. Journal of Physics: Conference Series. Jun 1;1940(1):012033. (2021)

43. Yue, Z., Economy, J.: 4 - Carbonization and activation for production of activated carbon fibers [Internet]. Chen JY, editor. ScienceDirect. Oxford: Woodhead Publishing; p. 61–139. Available from: (2017). https://www.sciencedirect.com/science/article/pii/B9780081006603000043
44. Yue, Z., Economy, J.: 4 - Carbonization and activation for production of activated carbon fibers [Internet]. Chen JY, editor. ScienceDirect. Oxford: Woodhead Publishing; p. 61–139. Available from: (2017). https://www.sciencedirect.com/science/article/pii/B9780081006603000043
45. Taer, E., Febriyanti, F., Apriwandi, Taslim, R., Agustino, Sinta Mustika, W.: Investigation of H_2SO_4 and KOH aqueous electrolytes on the electrochemical performance of activated carbon derived from areca catechu husk. Journal of Physics: Conference Series. Jun 1;1940(1):012033. (2021)
46. Donohue, M.D., Aranovich, G.L.: Classification of Gibbs adsorption isotherms. Advances in Colloid and Interface Science [Internet]. Available from: (1998). Jul;76–77:137–52 https://www.sciencedirect.com/science/article/pii/S000186869800044X
47. Chang, S.-S., Clair, B., Ruelle, J., Beauchene, J., Di Renzo, F., Quignard, F., et al.: Mesoporosity as a new parameter for understanding tension stress generation in trees. Journal of Experimental Botany. May 12;60(11):3023–30. (2009)
48. González, A., Goikolea, E., Barrena, J.A., Mysyk, R.: Review on supercapacitors: Technologies and materials. Renewable and Sustainable Energy Reviews [Internet]. Available from: (2016). May;58:1189–206 https://www.sciencedirect.com/science/article/pii/S1364032115016329
49. Scibioh, M.A., Viswanathan, B.: Fundamentals and energy storage mechanisms—overview.Materials for Supercapacitor Applications. ;15–33. (2020)
50. Marcuzzo, J.S., Cuña, A., Tancredi, N., Mendez, E., Bernardi, H.: Microporus activated carbon fiber felt from Brazilian textile PAN fiber: preparation, characterization and application as super capacitor electrode [Internet]. www.semanticscholar.org. 2016 [cited 2022 Dec 16]. Available from: https://www.semanticscholar.org/paper/Microporus-activated-carbon-fiber-felt-from-textile-Marcuzzo-Cu%C3%B1a/a8dd32f636bcf7439ab7c0f80e3fba881c3e4f24
51. Kurzweil, P.: Electrochemical Double-layer Capacitors.Electrochemical Energy Storage for Renewable Sources and Grid Balancing. ;345–407. (2015)
52. Chen, J.Y.: 1 - Introduction [Internet]. Chen JY, editor. ScienceDirect. Oxford: Woodhead Publishing; [cited 2022 Nov 22]. p. 3–20. Available from: (2017). https://www.sciencedirect.com/science/article/pii/B9780081006603000018
53. Yue, Z., Economy, J.: 4 - Carbonization and activation for production of activated carbon fibers [Internet]. Chen JY, editor. ScienceDirect. Oxford: Woodhead Publishing; p. 61–139. Available from: (2017). https://www.sciencedirect.com/science/article/pii/B9780081006603000043
54. Farnsworth, A., Chirima, G., Yu, F.: Raman Spectroscopy: A Key Technique in Investigating Carbon-Based Materials. Spectroscopy [Internet]. Aug 1 [cited 2022 Dec 15];36(8):9–14, 90–914, 90. Available from: (2021). https://www.spectroscopyonline.com/view/raman-spectroscopy-a-key-technique-in-investigating-carbon-based-materials

55. Barzegar, F., Momodu, D.Y., Fashedemi, O.O., Bello, A., Dangbegnon, J.K., Manyala, N.: Investigation of different aqueous electrolytes on the electrochemical performance of activated carbon-based supercapacitors. RSC Adv. **5**(130), 107482–107487 (2015)
56. Tyler, S., Mathis, N., Kurra, X., Wang, D., Pinto, P., Simon, et al.: Energy Storage Data Reporting in Perspective-Guidelines for Interpreting the Performance of Electrochemical Energy Storage Systems. Advanced Energy Materials, Wiley-VCH Verlag, 9 (39), pp.1902007. ff10.1002/aenm.201902007ff. (2019). ffhal-02519795
57. Castro-Gutiérrez, J., Celzard, A., Fierro, V.: Energy Storage in Supercapacitors: Focus on Tannin-Derived Carbon Electrodes.Frontiers in Materials. (2020). Jul 22;7.
58. Sagadevan, S., Marlinda, A.R., Chowdhury, Z.Z., Wahab, Y.B.A., Hamizi, N.A., Shahid, M.M., et al.: Fundamental electrochemical energy storage systems.Advances in Supercapacitor and Supercapattery. ;27–43. (2021)
59. Aziz, S.B., Hamsan, M.H., Brza, M.A., Kadir, M.F.Z., Muzakir, S.K., Abdulwahid, R.T.: Effect of glycerol on EDLC characteristics of chitosan:methylcellulose polymer blend electrolytes. J. Mater. Res. Technol. **9**(4), 8355–8366 (2020 Jul)
60. Scibioh, M.A., Viswanathan, B.: Fundamentals and energy storage mechanisms—overview.Materials for Supercapacitor Applications. ;15–33. (2020)
61. Scibioh, M.A., Viswanathan, B.: Characterization methods for supercapacitors.Materials for Supercapacitor Applications. ;315–72. (2020)
62. Wang, Y., Song, Y., Xia, Y.: Electrochemical capacitors: mechanism, materials, systems, characterization and applications. Chem. Soc. Rev. **45**(21), 5925–5950 (2016)
63. Rodrigues, A.C., da Silva, E.L., Quirino, S.F., Cuña, A., Marcuzzo, J.S., Matsushima, J.T., et al.: Ag@Activated Carbon Felt Composite as Electrode for Supercapacitors and a Study of Three Different Aqueous Electrolytes. Materials Research. Nov 8;22(1). (2018)
64. Rodrigues, A.C., Munhoz, M.G.C., Pinheiro, B.S., Batista, A.F., Amaral-Labat, G.A., Cuña, A., et al.: N-activated carbon fiber produced by oxidation process design and its application as supercapacitor electrode.Journal of Porous Materials. 2019 Aug28;27(1):141–9
65. Pal, B., Yang, S., Ramesh, S., Thangadurai, V., Jose, R.: Electrolyte selection for supercapacitive devices: a critical review. Nanoscale Adv. **1**(10), 3807–3835 (2019)
66. Scibioh, M.A., Viswanathan, B.: Characterization methods for supercapacitors.Materials for Supercapacitor Applications. ;315–72. (2020)
67. Scibioh, M.A., Viswanathan, B.: Characterization methods for supercapacitors.Materials for Supercapacitor Applications. ;315–72. (2020)
68. Castro-Gutiérrez, J., Celzard, A., Fierro, V.: Energy Storage in Supercapacitors: Focus on Tannin-Derived Carbon Electrodes.Frontiers in Materials. (2020). Jul 22;7.
69. Farma, R., Deraman, M., Talib, I.A.: Physical and Electrochemical Properties of Supercapacitor Electrodes Derived from Carbon Nanotube and Biomass Carbon. International Journal of

ELECTROCHEMICAL SCIENCE [Internet]. 8:257–73. Available from: http://www.electrochemsci.org/papers/vol8/80100257.pdf

70. Rodrigues, A.C., da Silva, E.L., Quirino, S.F., Cuña, A., Marcuzzo, J.S., Matsushima, J.T., et al.: Ag@Activated Carbon Felt Composite as Electrode for Supercapacitors and a Study of Three Different Aqueous Electrolytes. Materials Research. Nov 8;22(1). (2018)
71. Farma, R., Deraman, M., Talib, I.A.: Physical and Electrochemical Properties of Supercapacitor Electrodes Derived from Carbon Nanotube and Biomass Carbon. International Journal of ELECTROCHEMICAL SCIENCE [Internet]. 8:257–73. Available from: http://www.electrochemsci.org/papers/vol8/80100257.pdf
72. Chen, J., Lee, P.S.: Electrochemical Supercapacitors: From Mechanism Understanding to Multifunctional Applications. Advanced Energy Materials. Dec 21;11(6):2003311. (2020)
73. Barzegar, F., Momodu, D.Y., Fashedemi, O.O., Bello, A., Dangbegnon, J.K., Manyala, N.: Investigation of different aqueous electrolytes on the electrochemical performance of activated carbon-based supercapacitors. RSC Adv. **5**(130), 107482–107487 (2015)
74. Pal, B., Yang, S., Ramesh, S., Thangadurai, V., Jose, R.: Electrolyte selection for supercapacitive devices: a critical review. Nanoscale Adv. **1**(10), 3807–3835 (2019)
75. Zapata-Benabithe, Z., Diossa, G., Castro, C.D., Quintana, G.: Activated Carbon Bio-xerogels as Electrodes for Super Capacitors Applications. Procedia Eng. **148**, 18–24 (2016)
76. Castro-Gutiérrez, J., Celzard, A., Fierro, V.: Energy Storage in Supercapacitors: Focus on Tannin-Derived Carbon Electrodes.Frontiers in Materials. (2020). Jul 22;7.
77. Farma, R., Deraman, M., Talib, I.A.: Physical and Electrochemical Properties of Supercapacitor Electrodes Derived from Carbon Nanotube and Biomass Carbon. International Journal of ELECTROCHEMICAL SCIENCE [Internet]. 8:257–73. Available from: http://www.electrochemsci.org/papers/vol8/80100257.pdf
78. Scibioh, M.A., Viswanathan, B.: Characterization methods for supercapacitors.Materials for Supercapacitor Applications. ;315–72. (2020)
79. de Faria Junior, R.N.: Et al. Eletrólitos e eletrodos. In: Supercapacitor: conceitos básicos, materiais e métodos, pp. 47–74. Ed. Dos Autores, São Paulo (2021)
80. Aziz, S.B., Hamsan, M.H., Brza, M.A., Kadir, M.F.Z., Muzakir, S.K., Abdulwahid, R.T.: Effect of glycerol on EDLC characteristics of chitosan:methylcellulose polymer blend electrolytes. J. Mater. Res. Technol. **9**(4), 8355–8366 (2020 Jul)

Figures

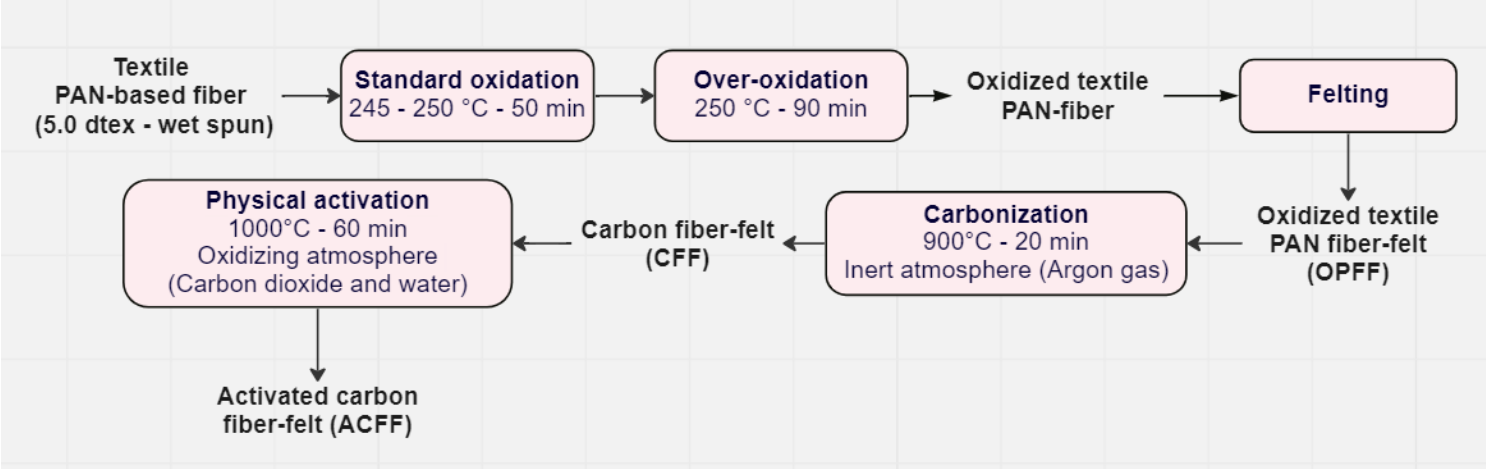

Figure 1

Synthesis of ACFF electrodes

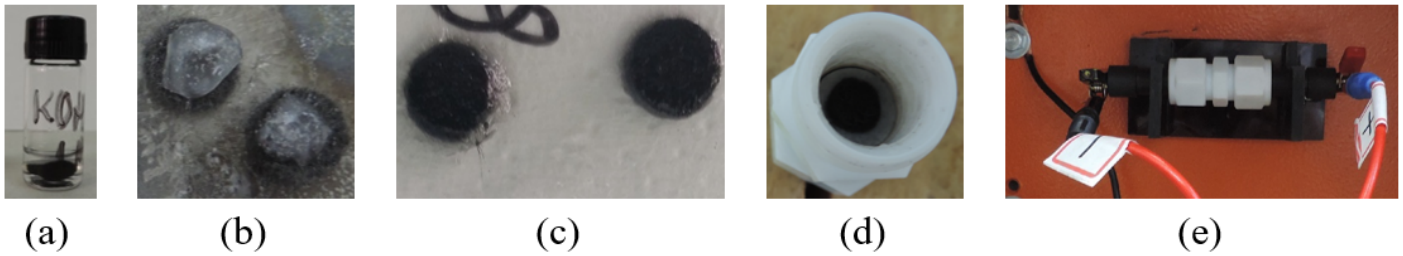

Figure 2

(a) aqueous-based electrolyte, (b) glycerol-based electrolyte before diffusion, (c) glycerol-based electrolyte after diffusion (d) interior view of Swagelok®-cell, and (e) assembled symmetric EDLC

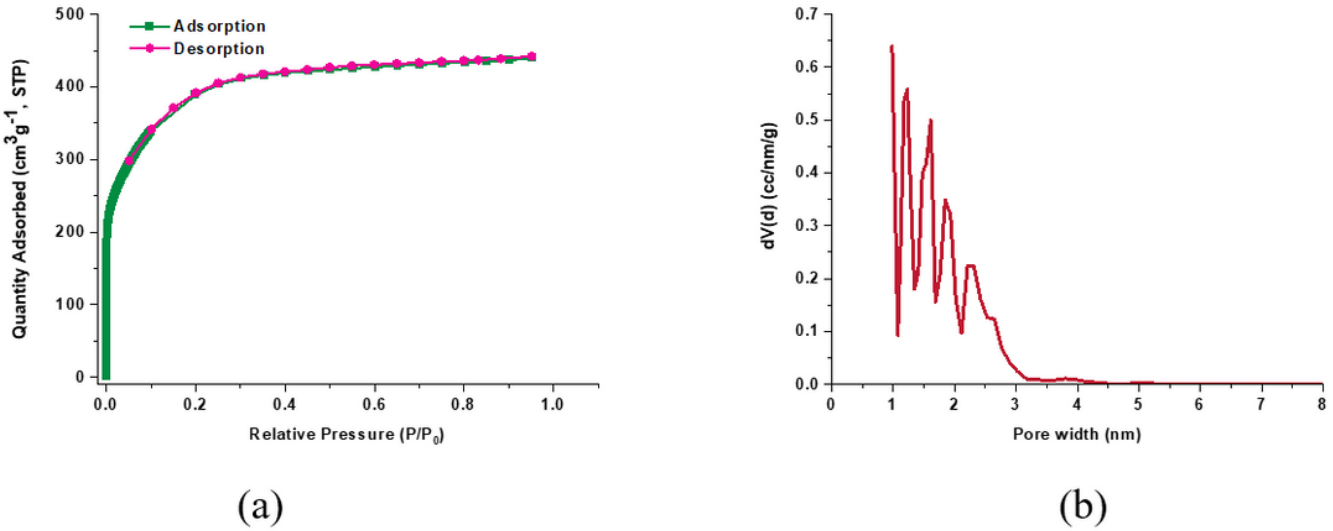

Figure 3

ACFF electrodes (a) nitrogen adsorption-desorption BET isotherm and (b) DFT pore size distribution.

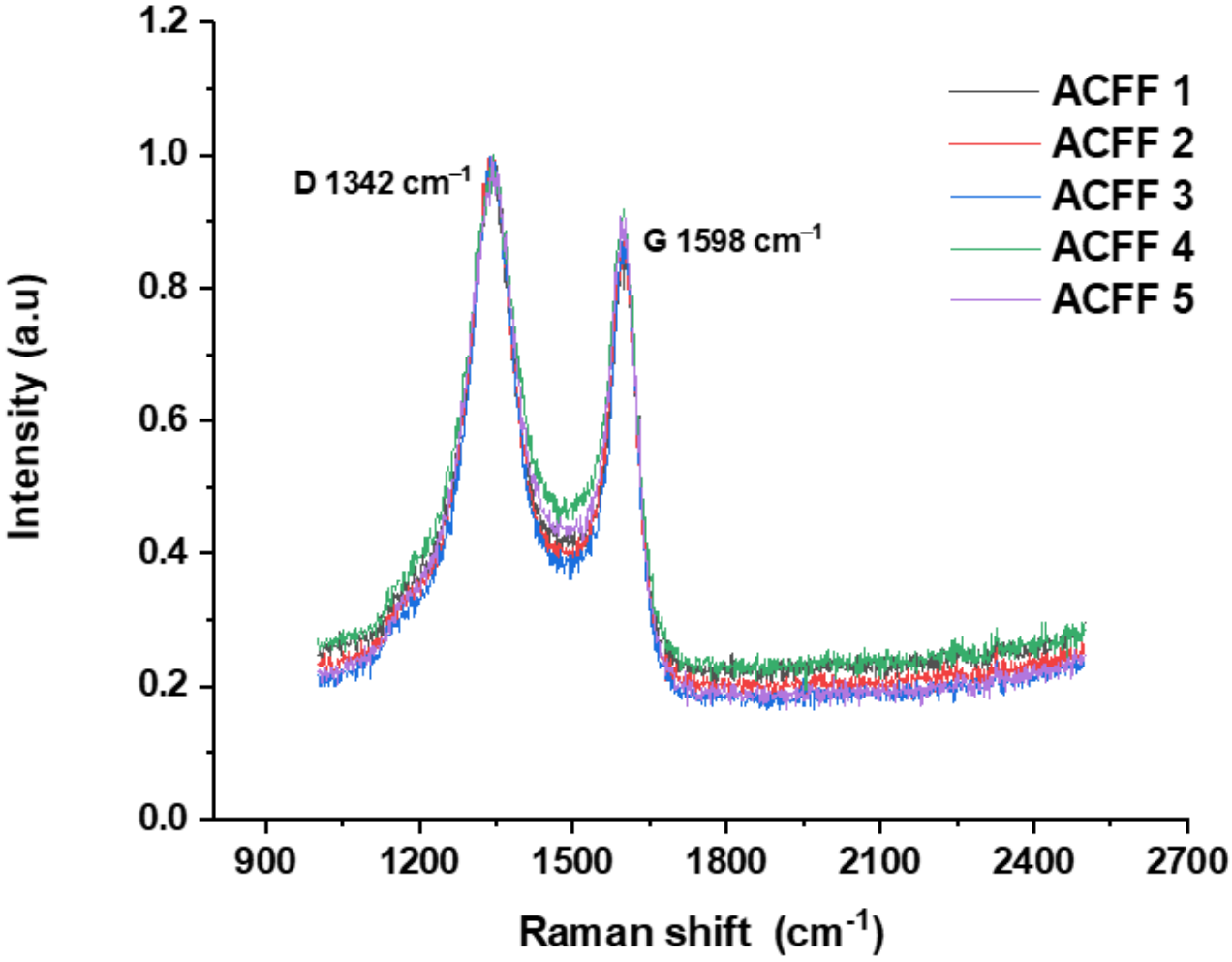

Figure 4

Raman spectra of ACFF electrodes

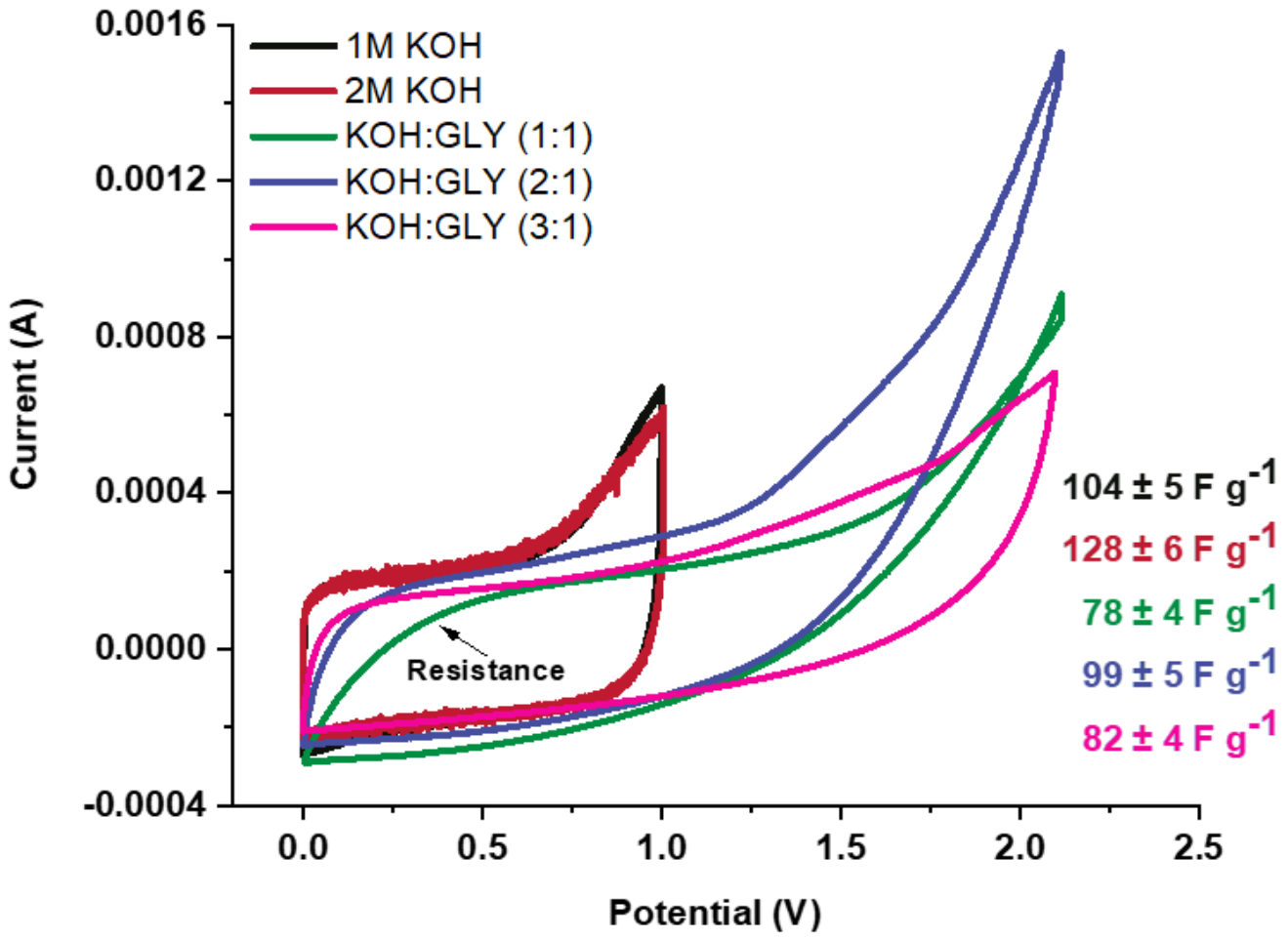

Figure 5

CV curves of ACFF-based EDLCs in aqueous-based and glycerol-based electrolytes at a scan rate of 1 mV s^{-1}

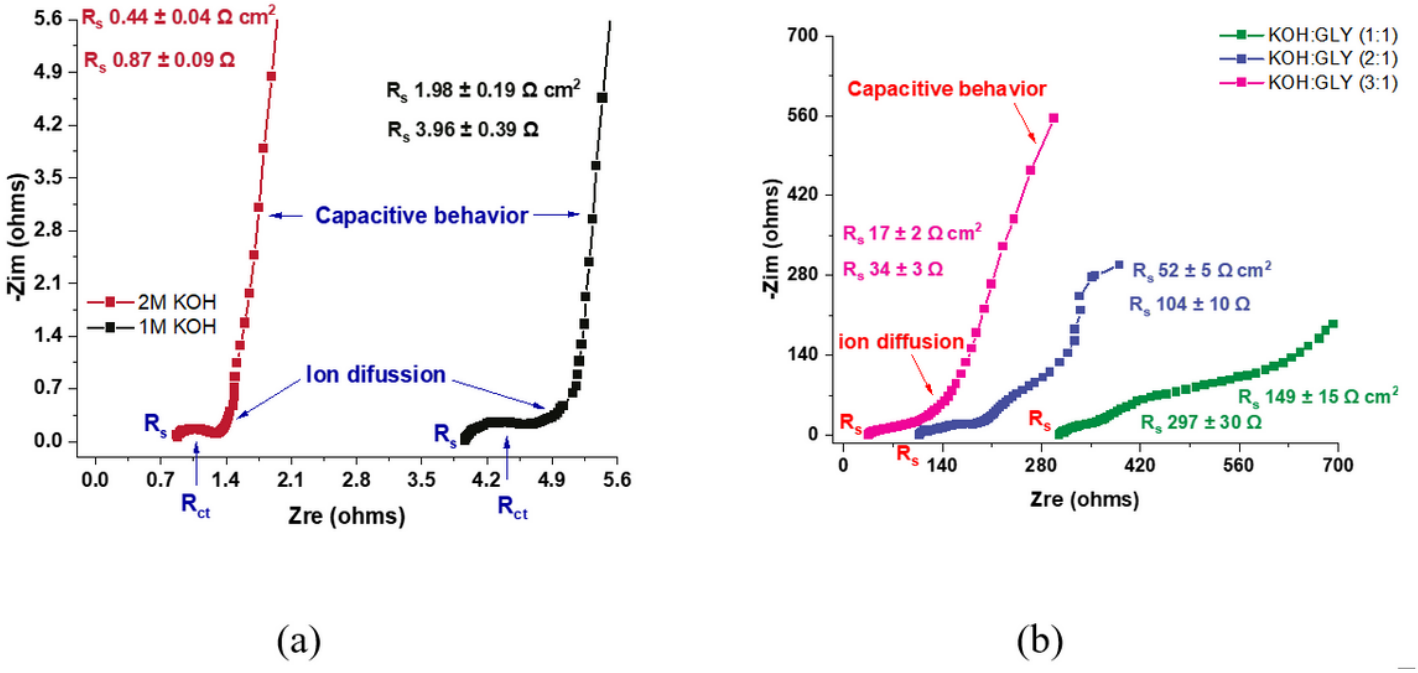

Figure 6

Nyquist plots of ACFF-based EDLCs (a) in aqueous-based electrolytes and (b) in glycerol-based electrolyte

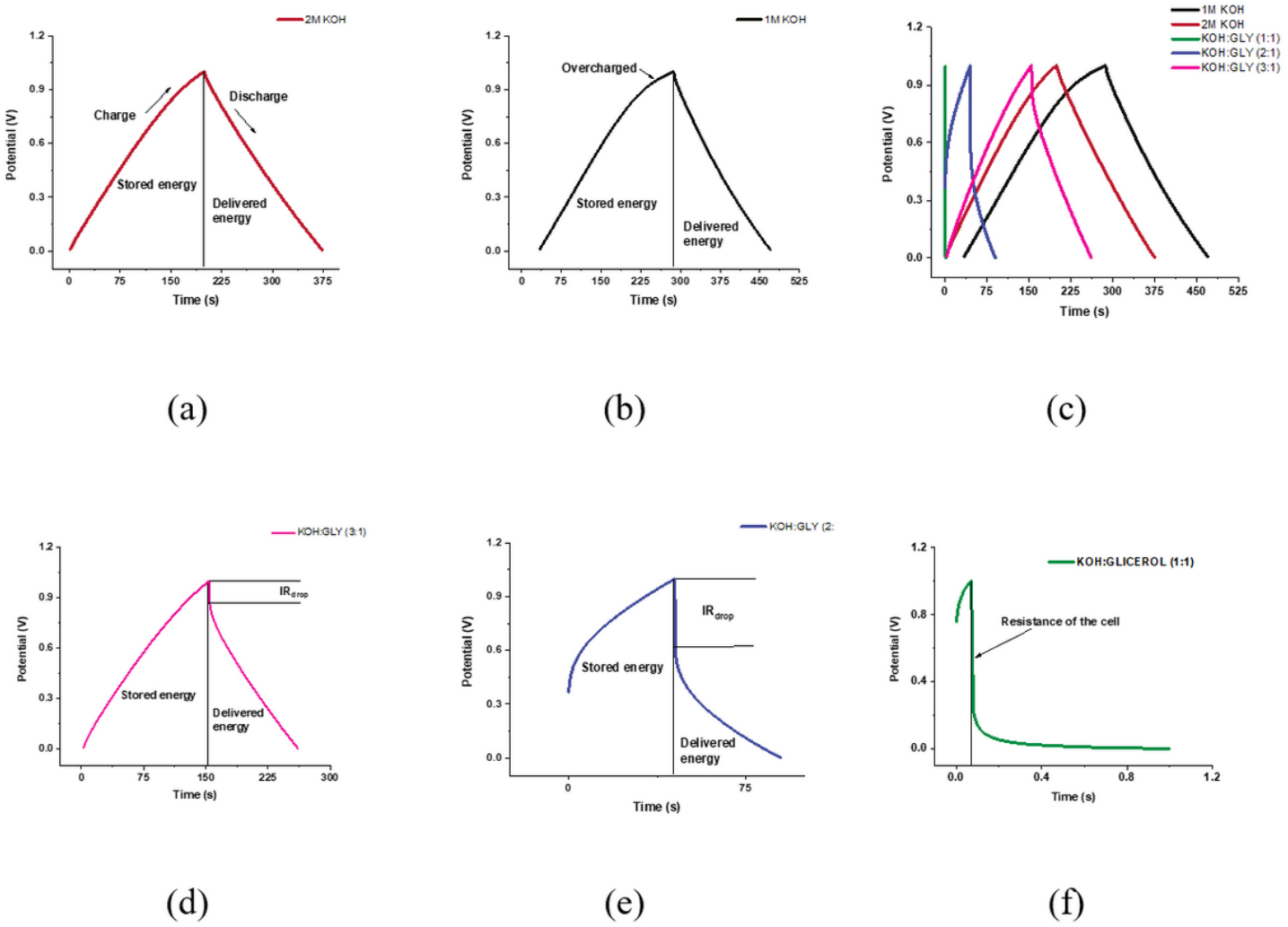

Figure 7

GCD curves of ACFF-based EDLCs at a current density of 0.15 A g^{-1} (a) and (b) in aqueous-based electrolytes (c) comparison, (d), (e) and (f) in glycerol-based electrolytes

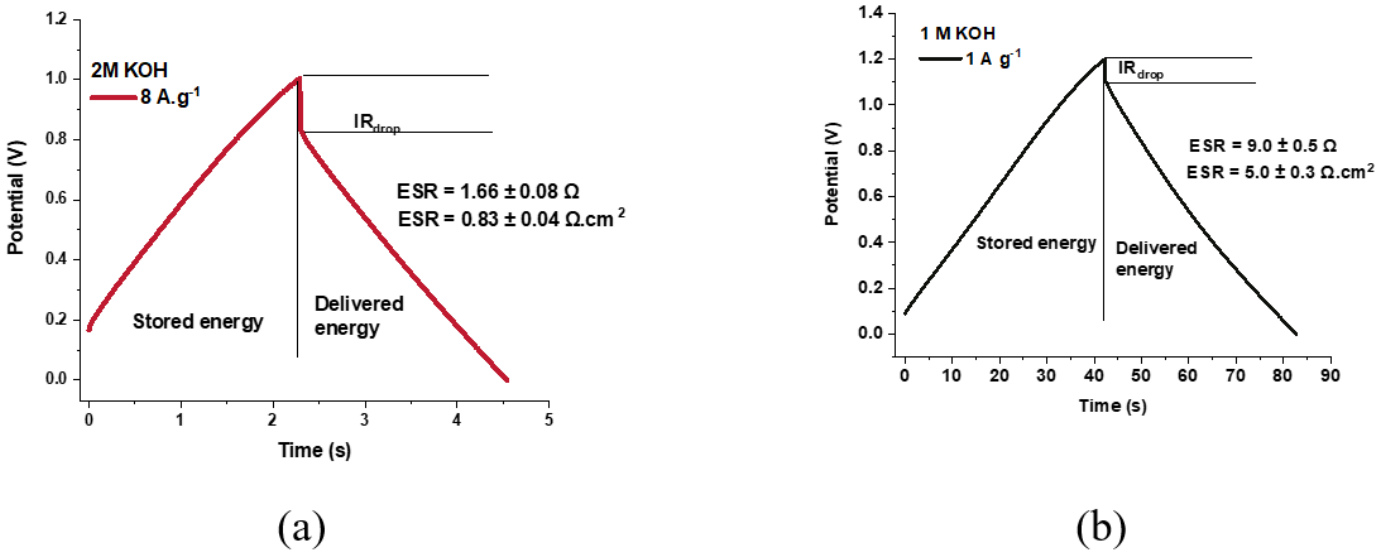

Figure 8

GCD curves of ACFF-based EDLCs in aqueous-based electrolytes at large current densities (a) 2 M KOH and (b) 1 M KOH

Supplementary Files

This is a list of supplementary files associated with this preprint. Click to download.

- AbstractWasteandBiomassValorization.jpg